

Turbulence in the highly restricted dynamics of a closure at second order: comparison with DNS

N C Constantinou¹, A Lozano-Durán², M-A Nikolaidis¹, B F Farrell³,
P J Ioannou¹, J Jiménez²

¹University of Athens, Department of Physics, Panepistimiopolis, Zografos, 15784 Athens, Greece

²School of Aeronautics, Universidad Politécnica de Madrid, 28040 Madrid, Spain

³Department of Earth and Planetary Sciences, Harvard University, Cambridge, MA 02138, USA

E-mail: navidcon@phys.uoa.gr

Abstract. S3T (Stochastic Structural Stability Theory) employs a closure at second order to obtain the dynamics of the statistical mean turbulent state. When S3T is implemented as a coupled set of equations for the streamwise mean and perturbation states, nonlinearity in the dynamics is restricted to interaction between the mean and perturbations. The S3T statistical mean state dynamics can be approximately implemented by similarly restricting the dynamics used in a direct numerical simulation (DNS) of the full Navier–Stokes equations (referred to as the NS system). Although this restricted nonlinear system (referred to as the RNL system) is greatly simplified in its dynamics in comparison to the associated NS, it nevertheless self-sustains a turbulent state in wall-bounded shear flow with structures and dynamics comparable to those observed in turbulence. Moreover, RNL turbulence can be analysed effectively using theoretical methods developed to study the closely related S3T system. In order to better understand RNL turbulence and its relation to NS turbulence, an extensive comparison is made of diagnostics of structure and dynamics in these systems. Although quantitative differences are found, the results show that turbulence in the RNL system closely parallels that in NS and suggest that the S3T/RNL system provides a promising reduced complexity model for studying turbulence in wall-bounded shear flows.

1. Introduction

The Navier–Stokes equations (NS), while comprising the complete dynamics of turbulence, have at least two disadvantages for theoretical investigation of the physics of turbulence: NS lacks analytical solution for the case of the fully turbulent state, and the nonlinear advection term results in turbulent states of high complexity that tend to obscure the fundamental mechanisms underlying the turbulence. One approach to overcoming these impediments has been the search for simplifications of NS that retain essential features of the turbulence dynamics. The Linearized Navier–Stokes equations (LNS) provide one example of the successful application of this approach in which the power of linear systems theory is made available to the study of turbulence [1, 2]. The LNS system captures the non-normal mechanism responsible for perturbation growth in NS [3]. This linear mechanism retained in LNS underlies both the process of subcritical transition to turbulence and the maintenance of the turbulent state [4–7]. However, linear models are unable to capture other essential phenomena in turbulence that are



intrinsically nonlinear, including the establishment of the turbulent mean velocity profile and the maintenance of turbulence in a statistically steady state in the absence of extrinsic excitation, the mechanism of which is referred to as the self-sustaining process (SSP). While there remain many further aspects of the turbulent state to be addressed, such as the structures and spectrum of the inertial subrange, a basis of understanding of wall turbulence comprises these fundamental aspects. One approach to studying these phenomena that has proven successful is to impose simplifications that isolate certain mechanisms of the turbulence dynamics. An example is restricting the size of the channel [8, 9]. The existence of the minimal channel for sustaining turbulence isolated the streak structure component of the SSP,¹ and showed that the SSP cycle comprises interactions among the streak, a pair of streamwise vortices of opposite sign (referred to as rolls) and the perturbation field. In minimal channel turbulence a single streak fits in the channel and the streamwise extent of the channel is of such length that the perturbations can adopt a structure allowing them to extract energy from the mean flow through a time dependent interaction [8, 10, 11]. Another example is imposing simplification of the dynamics by isolating specific regions of the turbulent flow. For example, it was found that when the inner and outer regions of the flow are isolated, turbulence was independently maintained in each region, arguing that an independent SSP is operating in these regions [11–13].

The minimal channel flow studies referred to above focused attention on the effort to obtain a self-consistent dynamical description of the interaction among the streak, the roll and the perturbation field. The streaks in minimal simulations are associated with the zero streamwise harmonic ($k_x = 0$). This observation motivates constructing a reduced complexity turbulence model based on the simplest closure of the LNS equations, which govern interaction between the streamwise mean flow (with the streak structure included) and the streamwise varying perturbation field (characterized by the $k_x \neq 0$ flow field). This system is obtained by augmenting LNS by only the nonlinearity resulting from including the feedback of the $k_x \neq 0$ perturbations on the $k_x = 0$ streamwise mean flow. This dynamics, which greatly restricts the nonlinearity of the NS, will be referred to as the restricted nonlinear system (RNL). Remarkably, as will be demonstrated in this work, the RNL self-sustains a realistic turbulent state, not only in minimal channels at low Reynolds numbers, but also in larger channels and at moderate Reynolds numbers.

The RNL system was introduced here as a simple extension of LNS that supports self-sustained turbulence. However, the RNL has deeper roots: it approximates the second-order cumulant closure of the NS, which is the basis of the Stochastic Structural Stability Theory (S3T). S3T defines a statistical mean state dynamical system, and implementations of this system have recently been used to develop theories of turbulence [14–20]. S3T employs an ensemble closure which produces autonomous statistical mean-state dynamics in which turbulent mean states exist as statistical equilibria. This makes the turbulent state available as an object for stability study, extending classical hydrodynamic stability theory, which addresses only the stability of stationary sample state solutions of the NS. In contrast, S3T can be used to determine the structural stability of statistical mean state entities such as attractors (characterised by a specific probability density function), so that for instance, when such an attractor becomes S3T-unstable the fluid state bifurcates to a new attractor characterized by a different probability density function. An example application of S3T is to a constant shear flow subjected to homogeneous turbulence excitation in which it is found that a bifurcation occurs when the Reynolds number exceeds a critical value resulting in a new stationary state comprising the mean flow with a roll-streak structure and a perturbation field supporting it in a new statistical steady state [7]. At an even higher Reynolds number a saddle-node bifurcation occurs in the S3T system, and the flow transitions to a time-dependent state that self-sustains, which is identified with transition to the

¹ In this context the term “streak” describes well-defined elongated regions of spanwise alternating bands of low and high speed fluid superimposed on the mean shear.

turbulent state. In the self-sustaining turbulent state the statistical mean state dynamics of S3T approaches the deterministic dynamics of the RNL. Recent work has exploited S3T dynamics to explore the role of streamwise coherent structures in turbulence, including the dynamics of the roll and streak structures [21, 22]. In this paper, we verify predictions of S3T for turbulence structure at high Reynolds numbers in pressure-driven channel flow by comparing flow statistics, structures, and dynamical diagnostics obtained from the RNL system to results obtained in the S3T system and to direct numerical simulations (DNS) of the full NS equations.

2. Modeling framework

Consider a pressure-driven plane Poiseuille flow maintained by application of the time-dependent pressure, $-G(t)x$, where x is the streamwise coordinate. The wall-normal direction is y and the spanwise direction is z . The lengths of the channel in the streamwise, wall-normal and spanwise direction are respectively L_x , $2h$ and L_z . The channel walls are at $y/h = 0$ and 2 . Streamwise mean, spanwise mean and time-mean quantities are denoted respectively by an overbar, $\overline{\bullet} = L_x^{-1} \int_0^{L_x} \bullet dx$, square brackets, $[\bullet] = L_z^{-1} \int_0^{L_z} \bullet dz$ and a wide hat $\widehat{\bullet} = T^{-1} \int_0^T \bullet dt$, with T sufficiently long. The velocity, \mathbf{u} , is decomposed into its streamwise mean value, denoted $\mathbf{U}(y, z, t)$, and the deviation from the mean (the perturbation), $\mathbf{u}'(x, y, z, t)$, so that the flow velocity is $\mathbf{u} = \mathbf{U} + \mathbf{u}'$. The pressure gradient is similarly written as $\nabla p = \nabla(-G(t)x + P(y, z, t) + p'(x, y, z, t))$. The NS can be then decomposed into an equation for the mean and an equation for the perturbation as follows:

$$\partial_t \mathbf{U} + \mathbf{U} \cdot \nabla \mathbf{U} - G(t)\hat{\mathbf{x}} + \nabla P - \nu \Delta \mathbf{U} = -\overline{\mathbf{u}' \cdot \nabla \mathbf{u}'}, \quad (1a)$$

$$\partial_t \mathbf{u}' + \mathbf{U} \cdot \nabla \mathbf{u}' + \mathbf{u}' \cdot \nabla \mathbf{U} + \nabla \mathbf{p}' - \nu \Delta \mathbf{u}' = -(\mathbf{u}' \cdot \nabla \mathbf{u}' - \overline{\mathbf{u}' \cdot \nabla \mathbf{u}'}) , \quad (1b)$$

$$\nabla \cdot \mathbf{U} = 0 , \quad \nabla \cdot \mathbf{u}' = 0 , \quad (1c)$$

where ν is the coefficient of kinematic viscosity. The x, y, z components of \mathbf{U} are (U, V, W) and the corresponding components of \mathbf{u}' are (u', v', w') . The streak component of the streamwise mean flow is denoted with U_s and defined as $U_s = U - [U]$. The V and W are the streamwise mean velocities of the roll vortices. Streamwise mean perturbation Reynolds stress components are therefore written as e.g. $\overline{u'u'}$, $\overline{u'v'}$.

The RNL approximation is obtained by neglecting the perturbation-perturbation interaction terms in Eq. (1b). The RNL system is:

$$\partial_t \mathbf{U} + \mathbf{U} \cdot \nabla \mathbf{U} - G(t)\hat{\mathbf{x}} + \nabla P - \nu \Delta \mathbf{U} = -\overline{\mathbf{u}' \cdot \nabla \mathbf{u}'}, \quad (2a)$$

$$\partial_t \mathbf{u}' + \mathbf{U} \cdot \nabla \mathbf{u}' + \mathbf{u}' \cdot \nabla \mathbf{U} + \nabla \mathbf{p}' - \nu \Delta \mathbf{u}' = 0 , \quad (2b)$$

$$\nabla \cdot \mathbf{U} = 0 , \quad \nabla \cdot \mathbf{u}' = 0 . \quad (2c)$$

Equation (2a) describes the dynamics of the streamwise mean flow, \mathbf{U} , which is driven by the divergence of the streamwise mean Reynolds stresses. These Reynolds stresses are obtained from Eq. (2b) which incorporates the influence of the time dependent streamwise mean flow $\mathbf{U}(y, z, t)$ on the streamwise varying perturbations \mathbf{u}' , but not the nonlinear interaction among the perturbations. Only the interaction of the perturbations directly on the streamwise mean flow, \mathbf{U} , is retained in the r.h.s. of Eq. (2a). Remarkably, RNL self-sustains turbulence by incorporating this one essential nonlinear interaction, in the absence of which a self-sustained turbulent state cannot be established [23, 24].

Table 1. Simulation parameters. $[L_x, L_z]/h$ is the domain size in the streamwise, spanwise direction. N_x, N_z are the number of Fourier components after dealiasing and N_y is the number of Chebyshev components. Re_τ is the Reynolds number of the simulation based on the friction velocity and $[L_x^+, L_z^+]$ is the channel size in wall units.

abbreviation	$[L_x, L_z]/h$	$N_x \times N_z \times N_y$	Re_τ	$[L_x^+, L_z^+]$
NS350	$[\pi, \pi]$	$128 \times 255 \times 193$	357.1	[1122, 1122]
RNL350	$[\pi, \pi]$	$128 \times 255 \times 193$	353.5	[1111, 1111]
NS950	$[\pi, \pi/2]$	$256 \times 255 \times 385$	939.9	[2953, 1476]
RNL950	$[\pi, \pi/2]$	$256 \times 255 \times 385$	882.4	[2772, 1386]

3. Numerical approach and simulation parameters

The data were obtained from a DNS of Eqs. (1) and from the RNL that is directly associated with the DNS. Both the DNS and its directly associated RNL are integrated with no-slip boundary conditions in the wall-normal direction and periodic boundary conditions in the streamwise and spanwise directions. The dynamics were expressed in the form of evolution equations for the wall-normal vorticity and the Laplacian of the wall-normal velocity, with spectral discretization and Fourier dealiasing in the two wall-parallel directions, and Chebychev polynomials in the wall-normal direction [25]. Time stepping was implemented using the third-order semi-implicit Runge-Kutta method.

Quantities reported in outer-units lengths are scaled by the channel half-width, h , and time by h/u_τ , and the corresponding Reynolds number is $Re_\tau = u_\tau h/\nu$ where $u_\tau = \sqrt{\nu dU/dy|_w}$ ($dU/dy|_w$ is the shear at the wall) is the friction velocity. Inner-units lengths are scaled by $h_\tau = Re_\tau^{-1}h$ and time by $Re_\tau^{-1}h/u_\tau$. Velocities scaled by the friction velocity u_τ will be denoted with the superscript +, which indicates inner-unit scaling.

4. Comparison of turbulence structure and dynamics diagnostics between NS and RNL

In this section we compare turbulence diagnostics obtained from self-sustained turbulence in the RNL system, Eqs. (2), to diagnostics obtained from the parallel DNS of the NS, Eqs. (1). The geometry and resolution of the NS and RNL cases are given in Table 1. Results are reported for Poiseuille turbulence at either $Re_\tau = 350$ or $Re_\tau = 950$. The RNL simulations were initialized with an NS state and run until a steady state was established. The RNL simulations produce self-sustained turbulence with the time mean estimated Re_τ values reported in Table 1, which are close to the Re_τ values of the NS turbulent state. Henceforth, the RNL simulations will be identified with the Re_τ value of the corresponding NS.

The turbulent mean profiles for the NS and RNL simulations with $Re_\tau = 350$ and $Re_\tau = 950$ are shown in outer variables in Fig. 1(a,c), while Fig. 1(b,d) shows the same data in inner-wall units. Previous simulations in Couette turbulence [22] at lower Reynolds numbers ($Re_\tau = 65$) showed very small differences between the mean turbulent profile in NS and RNL. These simulations at larger Reynolds numbers show significant differences in the mean turbulent profiles sustained by NS and RNL. This is especially pronounced in the outer regions, where RNL produces a mean turbulent profile with substantially smaller shear. Both profiles produce a logarithmic layer. However, the shear in these logarithmic regions are different: the von Kármán constant of NS at $Re_\tau = 950$ is $\kappa = 0.4$, while for RNL it is $\kappa = 0.77$. Formation of a logarithmic layer indicates that the underlying dynamics producing the logarithmic layer are retained in RNL. Because RNL maintains essentially the same stress and variance as NS in the logarithmic layer with a smaller shear, RNL is in this sense more efficient than NS in transferring

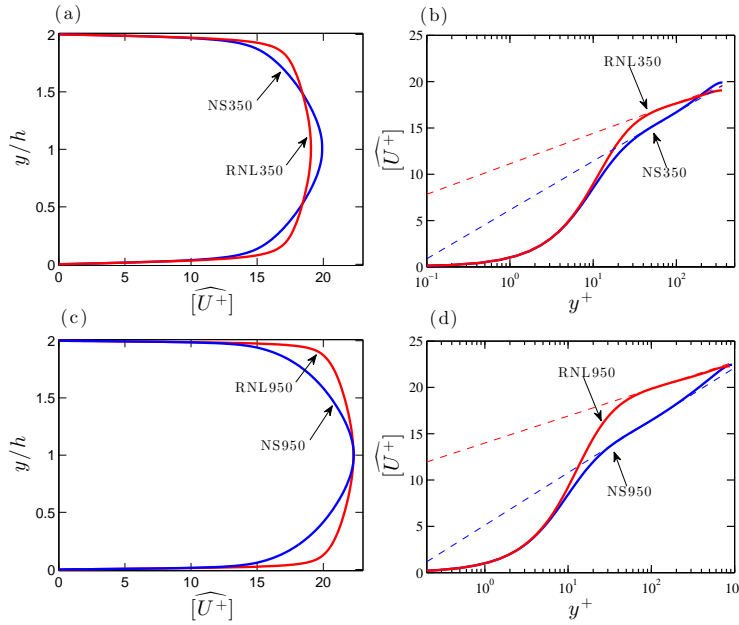


Figure 1. Streamwise velocity $[\overline{U^+}(y)]$ for the simulations in Table 1. (a) NS350 and RNL350 simulations, (c) NS950 and RNL950 simulations. The corresponding profiles are shown in (b) and (d) in wall units. The dashed lines indicate the best fit to the law of the wall, $[\overline{U^+}] = (1/\kappa) \log(y^+) + C$, with coefficients: NS350: $\kappa = 0.44$, $C = 6.1$, RNL350: $\kappa = 0.71$, $C = 11.1$, NS950: $\kappa = 0.40$, $C = 5.1$, RNL950: $\kappa = 0.77$, $C = 14.0$.

energy from the mean to the perturbations.

A comparison of perturbation statistics in RNL and NS is shown in Fig. 2 for $Re_\tau = 950$. The streamwise perturbation velocity fluctuations are significantly more pronounced in RNL, and the magnitude of the streak in RNL exceeds significantly the streak magnitude in NS in the inner wall region (cf. Fig. 2a). In contrast, the wall-normal and spanwise fluctuations in RNL are less pronounced than in NS (cf. Fig. 2b,c) and similarly the streak fluctuations in the outer

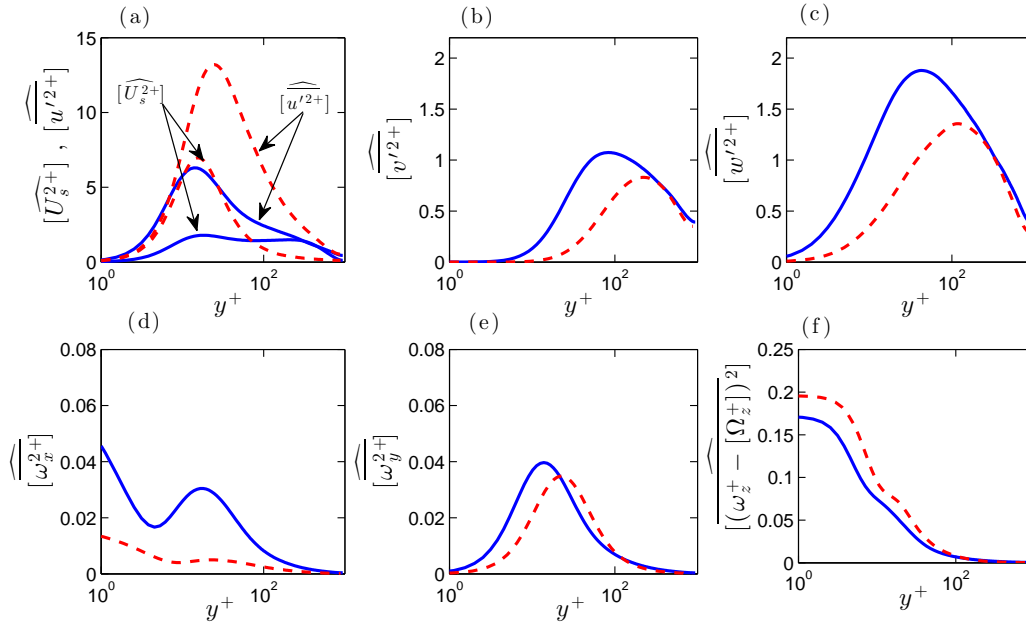


Figure 2. Comparison of velocity and vorticity fluctuations between NS950 and RNL950. Shown are (a) $[\overline{U_s^{2+}}]$, $[\overline{u'^{2+}}]$, (b) $[\overline{v'^{2+}}]$, (c) $[\overline{w'^{2+}}]$, (d) $[\overline{\omega_x^{2+}}]$, (e) $[\overline{\omega_y^{2+}}]$ and (f) $[\overline{(\omega_z^+ - [\Omega_z^+])^2}]$, where $\Omega_z^+ = -\partial U^+ / \partial y^+$ for the NS950 (solid) and RNL950 (dashed).

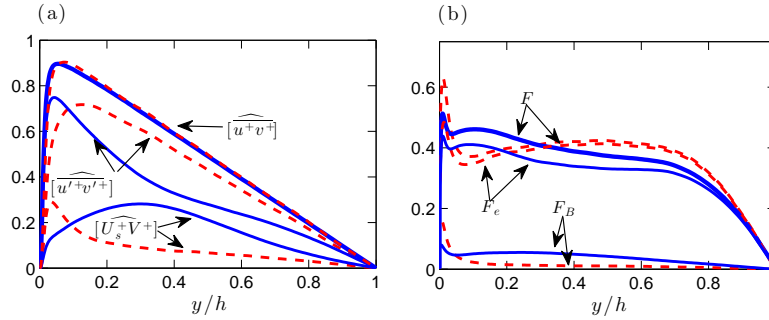


Figure 3. (a) The Reynolds stress component, $\widehat{uv}(y)$ in NS950 (solid) and in RNL950 (dashed). Also shown are each of the terms, $\widehat{U_s V}$ and $\widehat{u'v'}$ that sum to \widehat{uv} . Although the NS and RNL values of the total \widehat{uv} are almost identical, the contribution of $\widehat{U_s V}$ and $\widehat{u'v'}$ differ in NS and RNL. (b) Structure function, F , in NS950 (solid) and RNL950 (dashed). Shown are $F_B = -\widehat{UV} (\widehat{U^2} \widehat{V^2})^{-1/2}$, $F_e = -\widehat{u'v'} (\widehat{u'^2} \widehat{v'^2})^{-1/2}$ and $F = -\widehat{uv} (\widehat{u^2} \widehat{v^2})^{-1/2}$.

region are also less pronounced in RNL (cf. Fig. 2a). The structure of the fluctuations of the vorticity components as a function of y is shown in Fig. 2(d,e,f). The ω_z and ω_y fluctuations are similar in NS and RNL. The large ω_z fluctuations are associated with the shear of the streamwise velocity, while the ω_y fluctuations are associated with the streamwise streak structure. Only the ω_x fluctuations differ appreciably in amplitude between RNL and NS. This vorticity component is primarily associated with the fluctuations in the streamwise roll circulations, which are responsible for maintaining the streak, and which is central to sustaining the turbulence.

Despite this difference in the r.m.s. values of the velocity fluctuations, both RNL and NS produce very similar uv Reynolds stress. The increased amplitude of the velocity fluctuations in RNL is consistent with the fact that RNL and NS produce nearly the same energy dissipation rate. The Reynolds stress \widehat{uv} is the sum of $\widehat{U_s V}$ and $\widehat{u'v'}$. Comparison of the wall-normal distribution of the time mean of these two components of the Reynolds stress is shown in Fig. 3(a). Because the turbulence in NS and RNL is sustained with essentially the same pressure gradient, the sum of these Reynolds stresses is the same linear function of y outside the viscous layer. The Reynolds stress is dominated by the perturbation Reynolds stress $\widehat{u'v'}$ in both simulations, with the RNL stress penetrating farther from the wall. This is consistent with the fact that the perturbation structure in RNL has larger scale. This can be seen in a comparison of the NS and RNL perturbation structure shown in Fig. 4. Note that the Reynolds stress $\widehat{U_s V}$ associated with the streak and roll in the outer region of the NS simulation is larger than that in RNL. Further, the average correlation between the perturbation u' and v' fields are almost the same in both simulations, while the correlation between the U_s and V in the RNL is much smaller than that in NS in the outer layer. This is seen in a plot of the structure function (cf. [26]) shown in Fig. 3(b).

Turning now to the NS950 and RNL950 simulations, (y, z) -plane snapshots of the streamwise mean flow component (corresponding to $k_x = 0$ streamwise wavenumber) are shown in Fig. 5. Contours of the streamwise streak flow field, U_s , are shown together with vectors of the streamwise mean (V, W) field, which indicates the velocity components of the large-scale roll structure. The presence of organized streaks and associated rolls is evident both in the inner-wall and in the outer-wall region. Figure 6 shows a three-dimensional perspective of the flow of the NS and RNL simulations, in which all of the k_x components of the velocity field are included. Note that in the RNL there is no visual evidence of the $k_x = 0$ roll/streak structure which is required

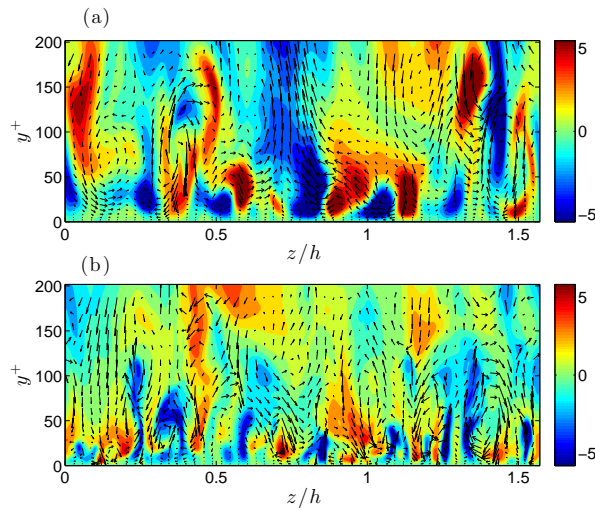


Figure 4. Perturbation structure, \mathbf{u}'^+ in (y, z) plane cross-section for (a) RNL950 and (b) NS950 in the inner wall region, $0 \leq y^+ \leq 200$. Both panels show contours of the u'^+ field, superimposed with components the (v'^+, w'^+) velocities.

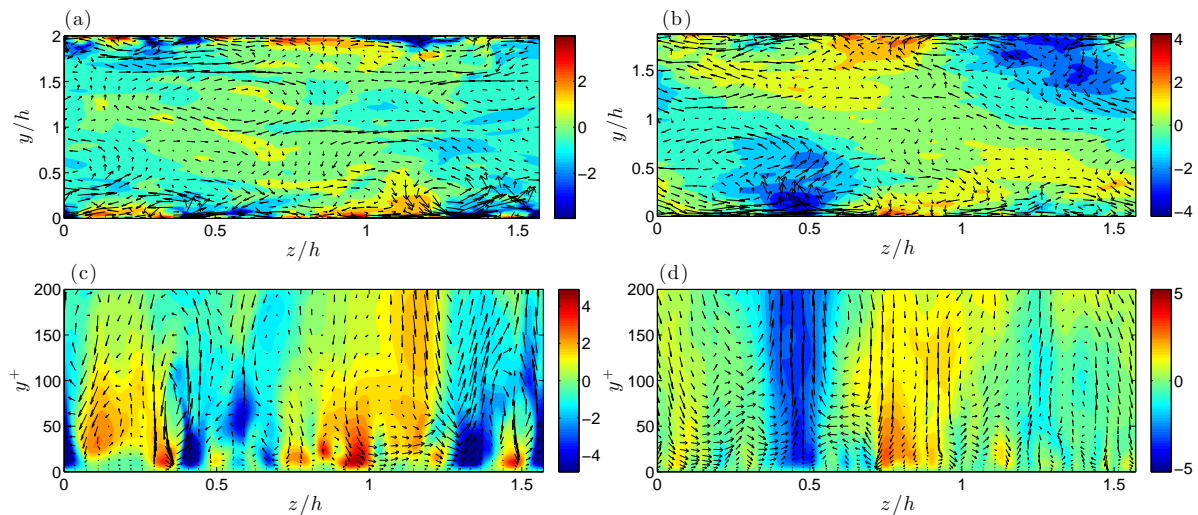


Figure 5. Instantaneous streamwise average flow velocity \mathbf{U}^+ (the $k_x = 0$ component of the flow) shown as a (y, z) plane cross-section for (a), (c) RNL950 and (b), (d) NS950. All panels show contours of the streak velocity, $U_s^+ = U^+ - [U^+]$, superimposed with the components of the (V^+, W^+) velocities. The top panels show the whole channel, while the bottom panels show the inner-wall region, $0 \leq y^+ \leq 200$.

by the restrictions of RNL dynamics to be the primary structure responsible for maintaining the RNL self-sustained turbulent state. Rather, the most energetic streamwise harmonic ($hk_x = 2$ for this channel) is most prominent and dominates the perturbation structure.

A comparison of the spectral energy densities of the velocity fields as a function of streamwise and spanwise wavenumber, (k_x, k_z) , provides an alternative view of the turbulent structure. The premultiplied spectral energy densities of each of the three contributions to the kinetic energy, E_{uu} , E_{vv} and E_{ww} at channel heights $y^+ = 20$, representative of the inner-wall region, and $y/h = 0.65$, representative of the outer-wall region, are shown in Fig. 7. Near the wall, RNL produces spanwise streak spacing and rolls similar to those in NS. The tendency of RNL to favor longer structure is also evident in these figures. The spectra for the outer region indicate a similar large-scale structure and good agreement in the spanwise spacing between RNL and NS. This figure establishes the presence of large-scale structure in the outer region in both RNL and NS. It has been noted that in NS, while the dominant large-scale structures scale linearly with distance from the wall in the inner-wall region, structures having the longest possible streamwise

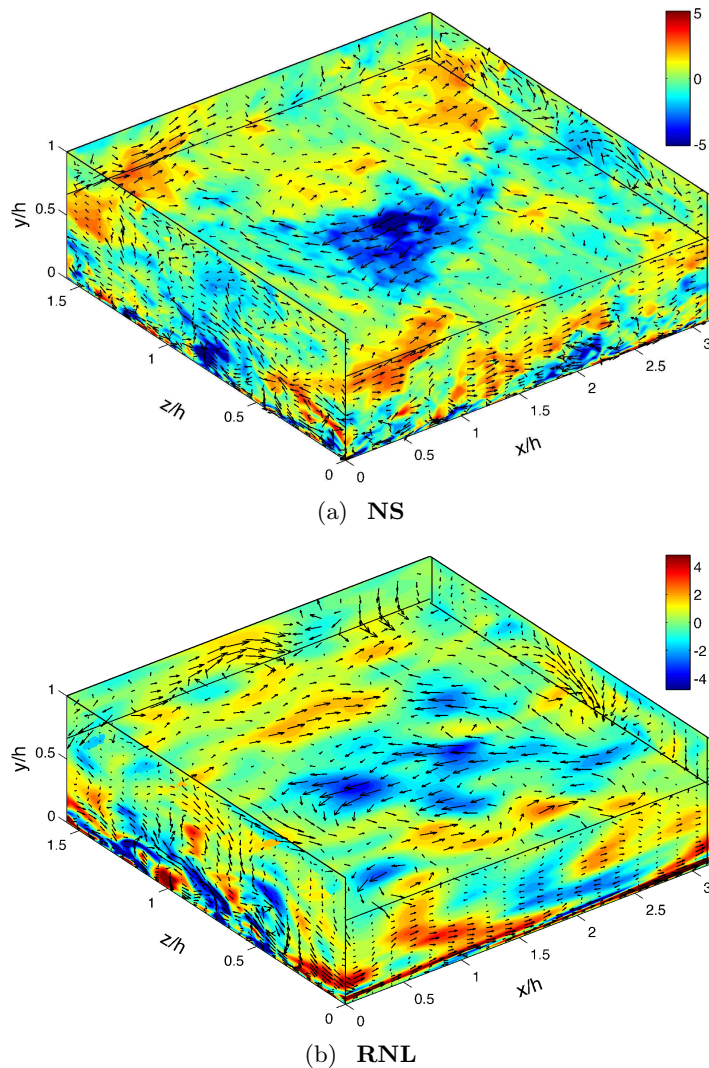


Figure 6. Three-dimensional perspective plots of the flow at a single time for (a) NS950, and (b) RNL950, for the lower half of the channel, $0 \leq y/h \leq 1$. Both images show contours of the streak component plus streamwise perturbation, $U_s^+ + u'^+$. The central x - z panel shows the flow at $y/h = 0.65$. The superimposed vectors represent the $(U_s^+ + u'^+, w^+)$ velocities for the x - z panel, $(U_s^+ + u'^+, v^+)$ velocities for the x - y panels and (v^+, w^+) velocities for the y - z panels. The parameters of the simulations are given in Table 1.

scale dominate the flow variance in the outer regions at high Reynolds number [27, 28]. This linear scaling near the wall can be seen in Fig. 8, where the pre-multiplied spectral densities are shown as a function of the distance y and of the spanwise wavelength, k_z , as in [27, 28], for both NL and RNL. In both simulations the spanwise wavelength associated with the spectral density maxima increases linearly with wall distance, and this linear dependence persists up to $y/h \approx 0.5$ (or $y^+ \approx 450$). Beyond $y/h \approx 0.5$ structures assume the widest wavelength allowed in the channel, suggesting that simulations must be performed in wider boxes in future work (cf. discussion in Jiménez & Hoyas [28] and Flores & Jiménez [29]). Corresponding contour plots of spectral energy density as a function of streamwise wavelength and wall-normal distance are shown in Fig. 9. These plots show that the perturbation variance in the inner wall and outer wall region is concentrated in a limited set of streamwise components which is apparent in Fig. 6. The restriction of the streamwise structure is particularly pronounced in the case of RNL, in which the outer layer variance peaks at $hk_x = 4$, which scale the wall-normal velocity inherits. Note that the longest wavelength in these graphs is equal to the streamwise length of the box, not to the infinite wavelength associated with the energy of the streak/roll structure, which, as we will see, is the most energetic structure in the NS but not in the RNL.

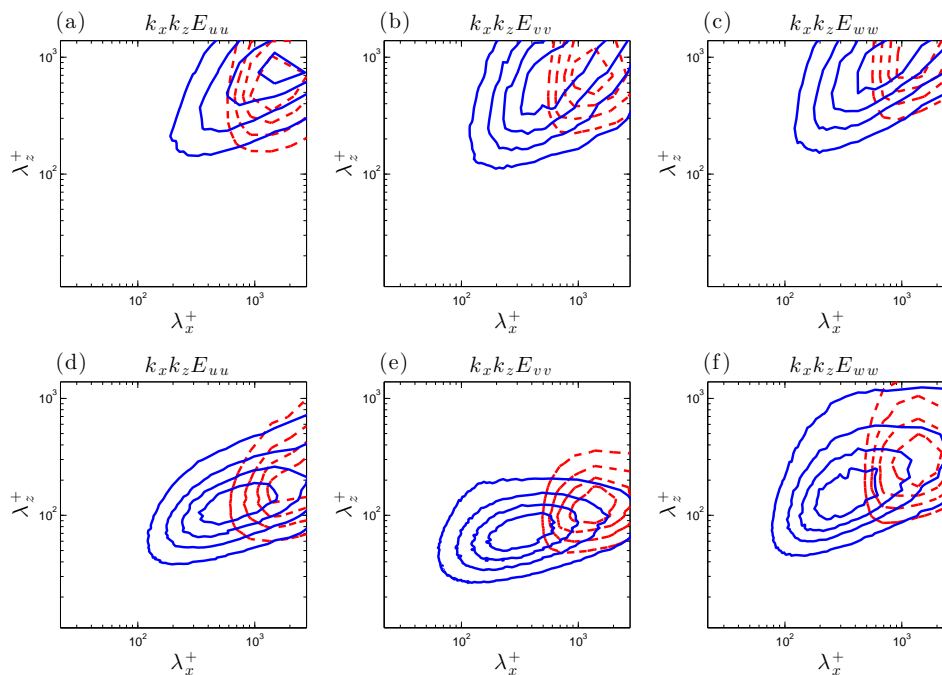


Figure 7. Contours of pre-multiplied power spectra $k_x k_z E_{ff}(k_x, k_z)$ with $f = u, v, w$, as a function of λ_x^+ and λ_z^+ for NS950 (solid) and RNL950 (dashed). (a), (b) and (c) show the spectral energy densities at wall distance $y/h = 0.65$ for the u , v and w respectively, while (d), (e) and (f) show the corresponding spectral energy densities at $y^+ = 20$. Contours are $(0.2, 0.4, 0.6, 0.8)$ times the maximum value of the corresponding spectrum. The maximum λ_x^+ and λ_z^+ are the lengths L_x^+ , L_z^+ of the periodic channel.

5. The RNL system as a minimal turbulence model

RNL turbulence has the property that, when initiated with full NS turbulence, it spontaneously transitions to a self-sustaining turbulent state supported by a severely restricted set of streamwise Fourier components. This property is consistent with the structure of the RNL system, which retains only the interaction between the $k_x = 0$ and the $k_x \neq 0$ components, from which it follows that the only energy source for maintaining a perturbation is its interaction with the mean flow [7]. It is remarkable that at these fairly high Reynolds numbers only a small set of streamwise harmonics are maintained by this interaction with the mean flow. Moreover, this is the fundamental interaction maintaining RNL turbulence and, by implication, given the similarity in the structure and dynamics between them, of NS turbulence as well. Even if the RNL dynamics is initialized with an NS flow state with energy in all N_x components, the RNL turbulence eventually reduces to involve only the $n_x \ll N_x$ Fourier components with wavenumber $hk_x = (2\pi/L_x) \times (0, 1, \dots, n_x - 1)$. We view this transition of NS turbulence to RNL turbulence as a process of distillation by which a small set of structures maintaining the turbulent state is identified, a result that was previously obtained in the case of self-sustained Couette turbulence at $Re = 400$ and $Re = 1000$ [7, 21]. In this previous work, a minimal-channel RNL simulation at $Re_\tau = 950$ was shown to self-sustain turbulence by the interaction of only two k_x components: $k_x = 0$ and the first harmonic in the channel. The analogous distillation process for the $Re_\tau = 950$ simulation is shown in Fig. 10(a). The time evolution of the energy of the first 15 streamwise varying Fourier components in an NS simulation is shown in the left part of the figure ($u_\tau t/h < 100$), while the subsequent evolution of these components is shown in the

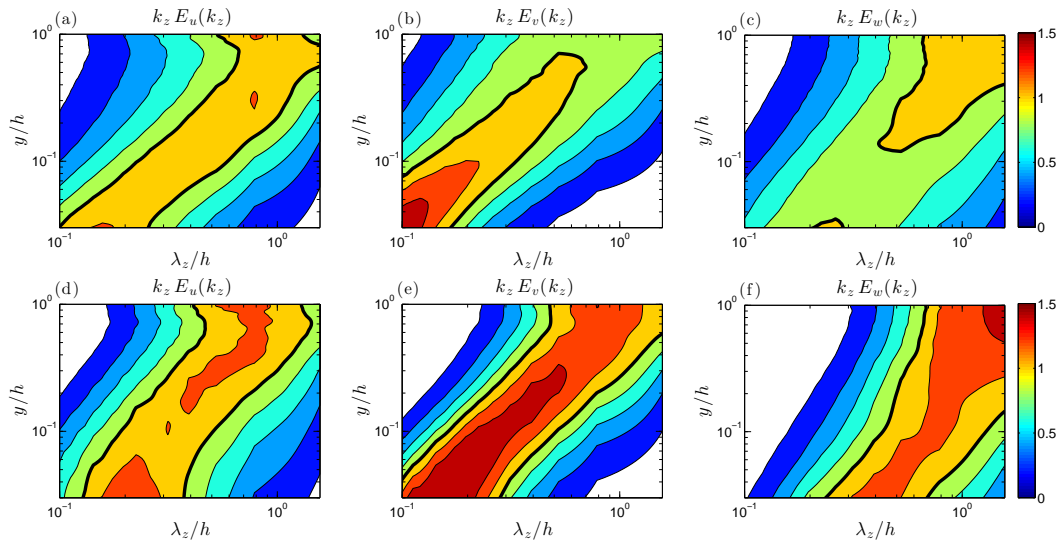


Figure 8. Normalized pre-multiplied spectral densities $k_z E_f(k_z) = k_z \sum_{k_x} E_{ff}(k_x, k_z)$, with $f = u, v, w$, as a function of spanwise wavelength, λ_z/h , and y/h . Spectral densities are normalized so that at each y the total energy, $\sum_{k_z} E_f(k_z)$, is the same. Shown are for NS950 (a) $k_z E_u(k_z)$, (b) $k_z E_v(k_z)$, (c) $k_z E_w(k_z)$ and for RNL950 (d) $k_z E_u(k_z)$, (e) $k_z E_v(k_z)$, (f) $k_z E_w(k_z)$. The isocontours are 0.2, 0.4, ..., 1.4, and the thicker line marks the 1.0 isocontour.

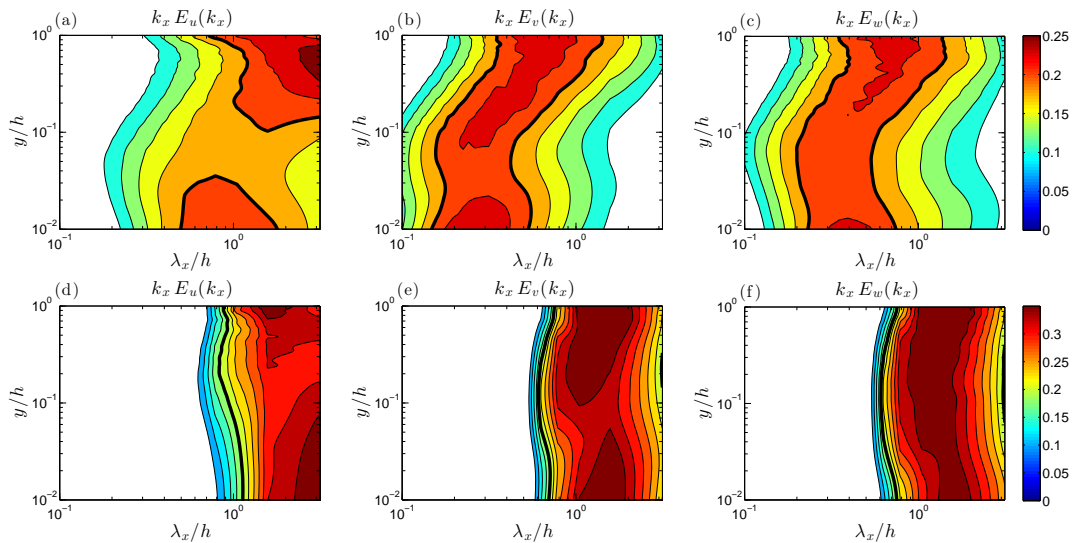


Figure 9. Normalized pre-multiplied spectral densities $k_x E_f(k_x) = k_x \sum_{k_z} E_{ff}(k_x, k_z)$, with $f = u, v, w$, as a function of streamwise wavelength, λ_x/h , and y/h . Spectral densities are normalized so that at each y the total energy, $\sum_{k_x} E_f(k_x)$, is the same. Shown are for NS950 (a) $k_x E_u(k_x)$, (b) $k_x E_v(k_x)$, (c) $k_x E_w(k_x)$ and for RNL950 (d) $k_x E_u(k_x)$, (e) $k_x E_v(k_x)$, (f) $k_x E_w(k_x)$. The isocontours are 0.1, 0.125, ..., 0.35, and the thicker line marks the 0.2 isocontour.

right part, after the perturbation-perturbation interactions are suppressed at the indicated time, so that the turbulence evolves under RNL dynamics. It is evident from Fig. 10(a) that RNL950 turbulence in a channel with $L_x = \pi h$ retains only the six Fourier components $hk_x = 2, 4, \dots, 12$ out of the $N_x = 127$ streamwise varying components that are present in the NS simulation. All components with $hk_x > 12$ decay exponentially. As a result, a transition occurs in which

a reduced-complexity dynamics maintaining turbulence arises, which self-sustains turbulence despite this greatly restricted support in streamwise wavenumber space. That RNL maintains a turbulent state similar to that of NS with nearly the same Re_τ ($Re_\tau = 882$ vs. $Re_\tau = 940$) implies that these systems have approximately the same energy production and dissipation and that the n_x components retained in RNL assume the burden of accounting for this energy production and dissipation. Specifically, the components in NS that are not retained in RNL are responsible for approximately one third of the total energy dissipation, which implies that the components that are retained in RNL must increase their dissipation by that much.

6. Streak structure dynamics in NS and RNL

Large scale roll/streak structures are prominent in the inner layer as well as in the outer layer, both in NS and in RNL. The dynamics of this structure can be diagnosed using the time

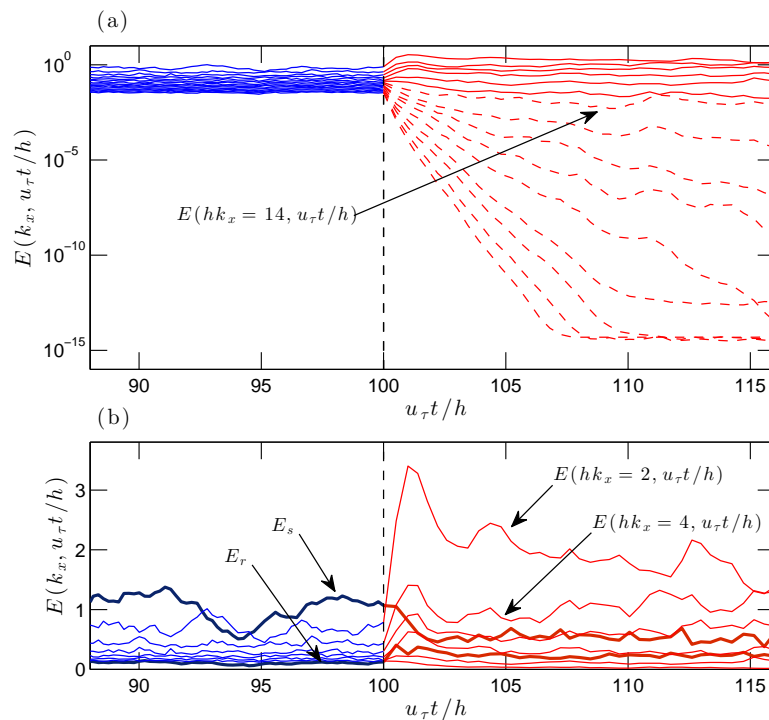


Figure 10. An NS950 simulation up to $u_\tau t/h = 100$ (indicated with the vertical line) is continued subsequently under RNL dynamics. Shown are (a) Energy of the first 15 streamwise varying Fourier components ($hk_x = 2, 4, \dots, 30$). The energy of the Fourier components decreases monotonically with wavenumber. Decaying Fourier components are indicated with dashed lines. After the transition to RNL dynamics all components with $hk_x \geq 14$ decay ($hk_x = 14$ decays, although it is not shown in this figure). Asymptotically the dynamics of the RNL950 turbulence is maintained by interaction between the set of surviving $hk_x = 2, 4, \dots, 12$ Fourier components and the mean flow ($k_x = 0$). (b) Detailed view showing the energy of the mean and surviving perturbation components during the transition from NS to RNL dynamics, in which the total energy increased by 10%. For the $k_x = 0$ shown are: the streak energy, $E_s = (hL_z)^{-1} \int dy dz U_s^{+2}/2$, and roll energy, $E_r = (hL_z)^{-1} \int dy dz (V^{+2} + W^{+2})/2$. The energy of the $hk_x = 2, 4, 6, 8$ components increases rapidly during the adjustment after transition to RNL dynamics. Note that the total energy in the perturbation $k_x \neq 0$ components decreases from 0.91 in the NS950 (0.56 being in the components that survive in the RNL) to 0.78 in RNL950. Also the roll/streak energy decreases from 1.1 in NS950 to 0.8 in RNL950, while the energy of the $k_x = k_z = 0$ component increases from 397 to 448.

evolution of the energy of each k_x component during the transition from NS to RNL, shown in Fig. 10(b). It can be seen that in NS the energy associated with the streamwise mean structure with $k_x = 0$ and $k_z \neq 0$ is dominant among the structures that deviate from the mean flow $[U]$. In the inner layer the interaction of roll/streak structures with the $k_x \neq 0$ perturbation field maintains turbulence through an SSP [7, 10, 11]. The RNL system provides an especially simple manifestation of this SSP, as its dynamics comprise only interactions between the mean ($k_x = 0$) and perturbation ($k_x \neq 0$) components. The fact that RNL self-sustains a counterpart turbulent state provides strong evidence that the RNL SSP captures the essential dynamics of turbulence in the inner-wall region.

The structure of the RNL system compels the interpretation that the time dependence of the SSP cycle, which might appear at first to consist of a concatenation of random and essentially unrelated events, is instead an intricate interaction dynamics among streaks, rolls and perturbations that produces the $\mathbf{U}(y, z, t)$ which, when introduced in Eq. (2b), results in the generation of an evolving perturbation Lyapunov structure with exactly zero Lyapunov exponent. S3T identifies this exquisitely contrived SSP cycle, which comprises the generation of the streak through lift-up by the rolls, and the maintenance of the rolls by torques induced by the perturbations which themselves are maintained by an essentially time-dependent parametric non-normal interaction with the streak (rather than e.g. inflectional instability of the streak structure) [7].

Vanishing of the Lyapunov exponent associated with the SSP is indicative of a feedback control process acting between the streaks and the perturbations by which the parametric instability of the perturbations on the time-dependent streak is reduced so that it asymptotically maintains a zero Lyapunov exponent. Examination of the transition from the NS to the RNL, shown by the simulation diagnostics in Fig. 10(b), reveals the action of this controller. When the interaction among the perturbations in Eq. (1b) is switched off so that the simulation is governed by RNL dynamics, we observe a sudden increase of the energy of the surviving $k_x \neq 0$ components, as shown by the rapid increase of the energy in the $hk_x = 2, 4, 6, 8$ components. An increase of the energy of these components is expected because the dissipative effect of the perturbation-perturbation nonlinearity that acts on these components is removed in RNL. As these modes grow, the SSP cycle quickly adjusts to a new turbulent equilibrium state characterized by reduced streak amplitude and increased energy in the largest streamwise scales. This SSP cycle is more efficient in the sense that a self-sustained turbulence with approximately the same Re_τ as that in NS is maintained with smaller mean shear. This turbulent state is dominated by high-amplitude fluctuations of the $hk_x = 2, 4, 6, 8$ components, as well as in the components associated with the wall-normal and spanwise direction. This can be seen in a comparison of the NS and RNL perturbation structure (the velocity field corresponding to $k_x \neq 0$) shown in Fig. 4. The perturbations in RNL simultaneously reduce the shear of the mean flow and maintain a reduced amplitude streak in the outer layer. A comparison of the shear, of the r.m.s. V velocity, and of the r.m.s. streak velocity, U_s , in the outer layer is shown as a function of y in Fig. 11, from which it can be seen that the reduction of the amplitude of the streak in RNL is equal to the reduction in the mean flow shear. It is important to note that these dependencies are integral to the SSP cycle, and specifically of its feedback control that determines the statistical steady state, and must be understood in the context of the cycle.

In the discussion above we have assumed that the presence of roll and streak structure in the outer layer in RNL indicates the existence of an SSP cycle there as well, and by implication also

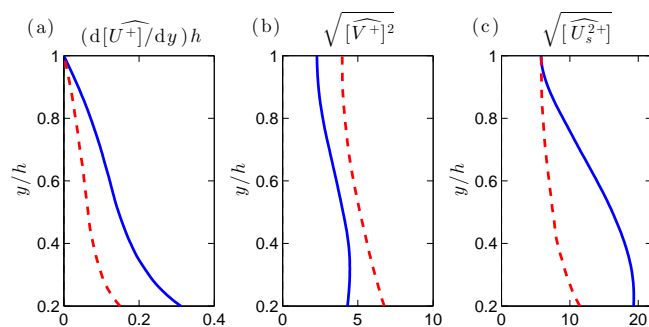


Figure 11. (a) Comparison of the turbulent mean shear, $(d[\widehat{U^+}]/dy)h$, (b) the r.m.s. of $[V^+]$, and (c) the r.m.s. of the streak velocity, U_s^+ , in the outer layer, $0.2 \leq y/h \leq 1$. NS950 (solid) and RNL950 (dashed).

in NS. In order to show this consider the momentum equation for the streamwise streak:

$$\partial_t U_s = - \underbrace{\left(V \partial_y U - [V \partial_y U] \right) - \left(W \partial_z U - [W \partial_z U] \right)}_A - \underbrace{\left(\overline{v' \partial_y u'} - [v' \partial_y u'] \right) - \left(\overline{w' \partial_z u'} - [w' \partial_z u'] \right)}_B + \nu \Delta U_s. \quad (3)$$

Term A in Eq. (3) is the contribution to the streak acceleration by the ‘lift-up’ mechanism and the ‘push-over’ mechanism, which represent transfer to streak momentum by the mean wall-normal and spanwise velocities respectively. Term B in Eq. (3) is the contribution to the streak momentum by the perturbation Reynolds stress divergence (structures with $k_x \neq 0$).

In order to identify the mechanism of streak maintenance we examine whether terms A and B accelerate or decelerate the streaks by evaluating from the simulation the contribution of the terms $I_A(t) = h^{-1} \int_R dy \mathcal{I}_A(y, t)$ and $I_B(t) = h^{-1} \int_R dy \mathcal{I}_B(y, t)$, where $\mathcal{I}_A(y, t) = hu_\tau^{-2} L_z^{-1} \int dz \text{sgn}(U_s) \times (\text{Term A})$ and $\mathcal{I}_B(y, t) = hu_\tau^{-2} L_z^{-1} \int dz \text{sgn}(U_s) \times (\text{Term B})$, to streak maintenance as a function of time and region R of the flow (similar results are obtained by multiplying with U_s to obtain an energy rather than a momentum budget for U_s). The results of this calculation are shown in Fig. 12 for R extending over the the inner region, the outer region and the whole channel. In the inner and outer wall regions for both NS and RNL the streak structure is supported primarily by the lift-up mechanism while the Reynolds stress divergences oppose the streak. While the magnitude of the acceleration by the lift-up and the deceleration by the Reynolds stress divergence are nearly the same in both NS and RNL in the inner region, in the outer region the acceleration by the lift-up in the RNL is about half of that in the NS, due to the smaller mean flow shear in RNL. The wall-normal structure of the time-mean $\widehat{\mathcal{I}}_A$ and $\widehat{\mathcal{I}}_B$ are shown in Fig. 13(a,b). We conclude that in NS and RNL the only positive contributions to the outer layer streaks are induced by the lift-up from the roll circulation, despite the small shear in this region. We next consider the dynamics maintaining the roll circulation.

7. Roll dynamics: maintenance of mean streamwise vorticity in NS and RNL

We have established that the roll circulation is not only responsible for streak maintenance in the inner layer but also in the outer layer. We now examine the mechanism of roll maintenance using streamwise averaged vorticity, $\Omega_x = \partial_y W - \partial_z V$, in the outer layer as a diagnostic. In order for roll circulation to be maintained against dissipation there must be a continuous generation of Ω_x . There are two possibilities for the maintenance of Ω_x in the outer layer: either Ω_x is generated locally in the outer layer, or it is advected from the near-wall region.

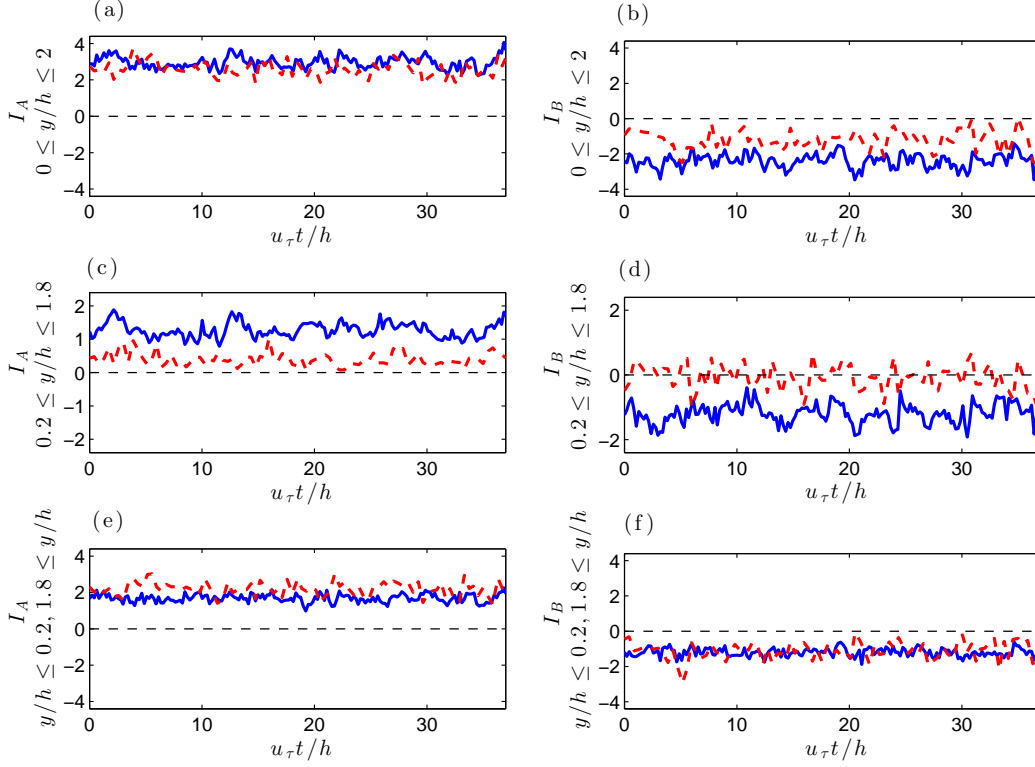


Figure 12. Streak-generation terms. (a) $I_A(t)$ over the whole channel with time-mean value 2.95 for NS950 and 2.59 for RNL950. (c) $I_A(t)$ over the outer region, $0.2 \leq y/h \leq 1.8$, with time-mean value 1.97 for NS950 and 0.4 for RNL950. (e) $I_A(t)$ over the inner region, $0 \leq y/h \leq 0.2$ $1.8 \leq y/h \leq 2$, with time-mean value 1.68 for NS950 and 2.19 for RNL950. (b) $I_B(t)$ over the whole channel with time-mean value -2.4 for NS950 and -1.21 for RNL950. (d) $I_B(t)$ over the outer region, $0.2 \leq y/h \leq 1.8$, with time-mean value -1.2 for NS950 and -0.08 for RNL950. (f) $I_B(t)$ over the inner region, $0 \leq y/h \leq 0.2$ $1.8 \leq y/h \leq 2$, with time-mean value -1.2 for NS950 and -1.13 for RNL950.

From Eq. (1a) we obtain that Ω_x satisfies the equation:

$$\partial_t \Omega_x = \underbrace{-V \partial_y \Omega_x - W \partial_z \Omega_x}_C + \underbrace{(\partial_{zz} - \partial_{yy}) (\overline{v'w'}) - \partial_{yz} (\overline{w'^2} - \overline{v'^2})}_D + \nu \Omega_x \Delta \Omega_x. \quad (4)$$

Term C expresses the streamwise vorticity tendency due to advection of Ω_x by the streamwise mean flow (V, W). Because there is no vortex stretching contribution to Ω_x from the (V, W) velocity field, this term only advects the Ω_x field and cannot sustain it against dissipation. However, this term may be responsible for systematic advection of Ω_x from the inner to the outer layer. Term D is the torque induced by the perturbation field. This is the only term that can maintain Ω_x . The overall budget for square streamwise vorticity in the region R , $y_1 \leq y \leq y_2$, $0 \leq z \leq L_z$, is given by:

$$\partial_t \int_{y_1}^{y_2} dy \left[\frac{1}{2} \Omega_x^2 \right] = - \underbrace{\left[\frac{1}{2} \Omega_x^2 V \right] \Big|_{y=y_1}^{y=y_2}}_{h^{-2} u_\tau^3 I_C} + \underbrace{\int_{y_1}^{y_2} dy \left[\Omega_x \times \text{Term D} \right]}_{h^{-2} u_\tau^3 I_D} + \nu \int_{y_1}^{y_2} dy \left[\Omega_x \Delta \Omega_x \right]. \quad (5)$$

where we have defined $I_C(t) = h^{-1} \int_R dy \mathcal{I}_C(y, t)$ and $I_D(t) = h^{-1} \int_R dy \mathcal{I}_D(y, t)$, with $\mathcal{I}_C(y, t) = h^3 u_\tau^{-3} L_z^{-1} \int dz \Omega_x \times (\text{Term C})$ and $\mathcal{I}_D(y, t) = h^3 u_\tau^{-3} L_z^{-1} \int dz \Omega_x \times (\text{Term D})$. Term

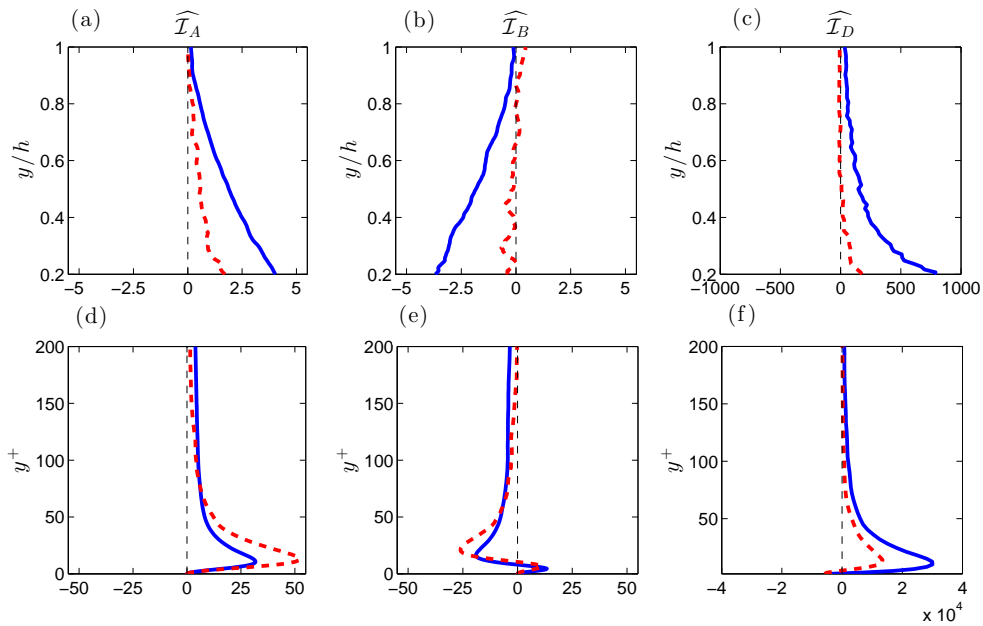


Figure 13. (a) Contribution to streak acceleration from the lift-up mechanism $\widehat{\mathcal{I}}_A$. (b) Contribution to streak acceleration from the perturbation Reynolds stress divergence $\widehat{\mathcal{I}}_B$. (c) Contribution to streamwise mean vorticity generation from perturbation Reynolds stress induced torques $\widehat{\mathcal{I}}_D$ (cf. section 7). Results from NS950 (solid) and RNL950 (dashed). Upper panels show structure in the outer layer, $0.2 \leq y/h \leq 1$, lower panels show the structure in the inner layer, $0 \leq y^+ \leq 200$.

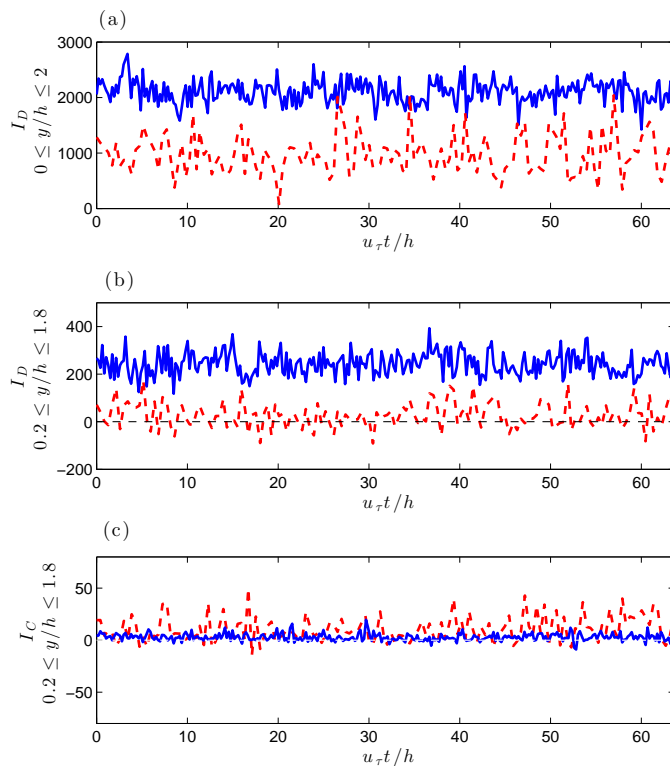


Figure 14. Time series of the contribution to the rate of change of $\int dy [\Omega_x^2/2]$ by perturbation torques, $I_D(t)$, and from advection of streamwise mean vorticity by the mean flow, $I_C(t)$, for NS950 (solid) and RNL950 (dashed). (a) I_D for the whole channel, $0 \leq y/h \leq 2$ ($I_C = 0$ in this case). The time-mean \widehat{I}_D is 2103.6 for NS950 and 982.8 for RNL950. (b) I_D over the outer layer, $0.2 \leq y/h \leq 1.8$. The time-mean \widehat{I}_D for this region is 242.5 for NS950 and only 28.7 for RNL950. (c) I_C for the outer layer $0.2 \leq y/h \leq 1.8$. The time-mean \widehat{I}_C is 2.9 for NS950 and 11.2 for RNL950. These figures show that in NS the roll is maintained locally by the perturbation Reynolds stresses and that in RNL the major contribution to the roll maintenance is contributed locally from perturbation induced torques.

I_C represents the flux of vorticity into the region by the streamwise averaged wall-normal velocity, V .

Time series of the contributions from $I_C(t)$ and $I_D(t)$ to the Ω_x production for NS950 and RNL950, shown in Fig. 14, demonstrate that Ω_x is primarily generated in situ by Reynolds stress torques. The corresponding wall-normal structure of the time-mean \widehat{I}_D , representing the local contribution to streamwise mean vorticity generation from perturbation Reynolds stress induced torques is shown in Fig. 13(c). Note that for NS in the outer layer, the streamwise mean vorticity generation by the Reynolds stress is strongly positive at each instant. This is so despite the fact that the r.m.s. V velocity is smaller in the NS than in the RNL, as seen in Fig. 11, implying greater streamwise vorticity dissipation in the NS. It could be argued that the positive value of the generation I_D found in NS and RNL is a consequence of the finite streamwise extent of the channel and as the channel length increases, assuming that there is no systematic correlation between streamwise average torques and streak structure, I_D should decrease as $1/\sqrt{L_x}$ and in the limit of an infinite channel the NS and RNL should sustain no Ω_x . However, S3T theory shows that there is a systematic correlation between streaks and roll generation by the perturbation torque resulting from the deformation of the turbulence by the streak and, as a result, it predicts that in the limit $L_x \rightarrow \infty$, I_D should asymptote to a finite non-zero value at least in RNL.

Having established that the streamwise vorticity in the outer layer is generated in situ from local Reynolds stress divergences we conclude that the SSP cycle is operational in the outer layer, just as in the inner one.

8. Discussion and Conclusions

We have established that RNL self-sustains turbulence at moderate Reynolds numbers in pressure-driven channel flow, despite its greatly simplified dynamics when compared to NS. Remarkably, in the RNL system, the turbulent state is maintained by a small set of structures with low streamwise wavenumber Fourier components (at $Re_\tau = 950$ with the chosen channel the SSP involves only the $k_x = 0$ streamwise mean and the next six streamwise Fourier components). Not only that, but this minimal turbulent dynamics arises spontaneously when the RNL system is initialized by NS turbulence at the same Reynolds number. In this way RNL spontaneously produces a turbulent state of reduced complexity. RNL identifies an exquisitely contrived SSP cycle which has been previously identified to comprise the generation of the streak through lift-up by the rolls, and the maintenance of the rolls by torques induced by the perturbations which themselves are maintained by an essentially time-dependent parametric non-normal interaction with the streak (rather than e.g. inflectional instability of the streak structure) [7]. The vanishing of the Lyapunov exponent associated with the SSP is indicative of a feedback control process acting between the streaks and the perturbations by which the parametric instability that sustains the perturbations on the time dependent streak is reduced to zero Lyapunov exponent, so that the turbulence neither diverges nor decays.

We have established that both NS and RNL produce a roll/streak structure in the outer layer and that an SSP is operating there despite the low shear in this region. It has been shown elsewhere that turbulence self-sustains in the logarithmic layer in the absence of boundaries [13]. This is consistent with our finding that an SSP cycle exists in both the inner-layer and outer-layer.

The turbulence maintained in RNL is closely related to its associated NS turbulence, and both exhibit a logarithmic layer, although with substantially different von Kármán constants. Existence of a logarithmic layer is a fundamental requirement of asymptotic matching between regions with different spatial scaling, as was noted by Millikan [30]. However, the exact value of the von Kármán constant does not have a similar fundamental basis in analysis, and RNL turbulence, which is closely related to NS turbulence but more efficient in producing Reynolds

stress, maintains as a consequence a smaller shear and therefore greater von Kármán constant. Specifically, we have determined that the SSP cycle in RNL is characterized by a more energetic and larger-scale perturbation structure, despite having a lower amplitude streak and mean shear.

Formation of roll/streak structures in the logarithmic layer is consistent with the universal mechanism by which turbulence is modified by the presence of a streak in such way as to induce growth of a roll structure configured to lead to continued growth of the original streak. This growth process underlies the non-normal parametric mechanism of maintaining the perturbation variance in the SSP that maintains turbulence if the Reynolds number is large enough [7]. This universal mechanism does not predict nor requires that the roll/streak structures be of finite streamwise extent and, in its simplest form, it has been demonstrated that it supports roll/streak structures with zero streamwise wavenumber. From this point of view, the observed length of roll/streak structures is not a consequence of the primary mechanism of the SSP supporting them, but rather a secondary effect of disruption by the turbulence. In this work we have provided evidence that NS turbulence is persuasively related in its dynamics to RNL turbulence. Moreover, given that the dynamics of RNL turbulence can be understood fundamentally from its direct relation with S3T turbulence, we conclude that the mechanism of turbulence in wall-bounded shear flow is the roll/streak/perturbation SSP that was previously identified to maintain S3T turbulence.

Acknowledgments

This work was funded in part by the Multiflow program of the European Research Council. Navid Constantinou acknowledges the support of the Alexander S. Onassis Public Benefit Foundation. Brian Farrell was supported by NSF AGS-1246929. We thank Dennice Gayme for helpful reviewing comments.

References

- [1] Farrell B F and Ioannou P J 1996 Generalized stability. Part I: Autonomous operators *J. Atmos. Sci.* **53** 2025–40
- [2] Farrell B F and Ioannou P J 1996 Generalized stability. Part II: Non-autonomous operators *J. Atmos. Sci.* **53** 2041–53
- [3] Henningson D S 1996 Comment on “Transition in shear flows. Nonlinear normality versus non-normal linearity” [Phys. Fluids **7**, 3060 (1995)] *Phys. Fluids* **8** 2257–58
- [4] Butler K M and Farrell B F 1992 Three-dimensional optimal perturbations in viscous shear flows *Phys. Fluids* **4** 1637–50
- [5] Henningson D S and Reddy S C 1994 On the role of linear mechanisms in transition to turbulence *Phys. Fluids* **6** 1396–98
- [6] Farrell B F and Ioannou P J 1994 Variance maintained by stochastic forcing of non-normal dynamical systems associated with linearly stable shear flows *Phys. Rev. Lett.* **72** 1118–91
- [7] Farrell B F and Ioannou P J 2012 Dynamics of streamwise rolls and streaks in turbulent wall-bounded shear flow *J. Fluid Mech.* **708** 149–96
- [8] Jiménez J and Moin P 1991 The minimal flow unit in near-wall turbulence *J. Fluid Mech.* **225** 213–40
- [9] Toh S and Itano T 2005 Interaction between a large-scale structure and near-wall structures in channel flow *J. Fluid Mech.* **524** 249–62
- [10] Hamilton K, Kim J and Waleffe F 1995 Regeneration Mechanisms of Near-Wall Turbulence Structures *J. Fluid Mech.* **287** 317–48
- [11] Jiménez J and Pinelli A 1999 The autonomous cycle of near-wall turbulence *J. Fluid Mech.* **389** 335–59
- [12] Tuerke F and Jiménez J 2013 Simulations of turbulent channels with prescribed velocity profiles *J. Fluid Mech.* **723** 587–603
- [13] Mizuno Y and Jiménez J 2013 Wall turbulence without walls *J. Fluid Mech.* **723** 429–55
- [14] Farrell B F and Ioannou P J 2003 Structural stability of turbulent jets *J. Atmos. Sci.* **60** 2101–18
- [15] Farrell B F and Ioannou P J 2007 Structure and spacing of jets in barotropic turbulence *J. Atmos. Sci.* **64** 3652–65
- [16] Marston J B, Conover E and Schneider T 2008 Statistics of an unstable barotropic jet from a cumulant expansion *J. Atmos. Sci.* **65** 1955–66

- [17] Tobias S M, Dagon K and Marston J B 2011 Astrophysical fluid dynamics via direct statistical simulations *Astrophys. J.* **727** 127
- [18] Srinivasan K and Young W R 2012 Zonostrophic instability *J. Atmos. Sci.* **69** 1633–56
- [19] Bakas N A and Ioannou P J 2013 Emergence of large scale structure in barotropic β -plane turbulence *Phys. Rev. Lett.* **110**(22) 224501
- [20] Constantinou N C, Farrell B F and Ioannou P J 2013 Emergence and equilibration of jets in beta-plane turbulence: applications of Stochastic Structural Stability Theory *J. Atmos. Sci.* Doi:10.1175/JAS-D-13-076.1, in press
- [21] Farrell B F, Gayme D F, Ioannou P J, Lieu B K and Jovanović M R 2012 Dynamics of the roll and streak structure in transition and turbulence *Proc. CTR Summer Program* (Stanford University) 43–54
- [22] Thomas V, Lieu B K, Jovanović M R, Farrell B F, Ioannou P J and Gayme D F 2014 Self-sustaining turbulence in the RNL system *Phys. Fluids* (submitted)
- [23] Gayme D F 2010 *A robust control approach to understanding nonlinear mechanisms in shear flow turbulence* Ph.D. thesis Caltech, Pasadena, CA, USA
- [24] Gayme D F, McKeon B J, Papachristodoulou A, Bamieh B and Doyle J C 2010 A streamwise constant model of turbulence in plane Couette flow *J. Fluid Mech.* **665** 99–119
- [25] Kim J, Moin P and Moser R 1987 Turbulence statistics in fully developed channel flow at low Reynolds number *J. Fluid Mech.* **177** 133–66
- [26] Flores O and Jiménez J 2006 Effect of wall-boundary disturbances on turbulent channel flows *J. Fluid Mech.* **566** 357–76
- [27] Jiménez J 1998 The largest scales of turbulent wall flows *CTR Ann. Res. Briefs* (Stanford University) 137–54
- [28] Jiménez J and Hoyas S 2008 Turbulent fluctuations above the buffer layer of wall-bounded flows *J. Fluid Mech.* **611** 215–36
- [29] Flores O and Jiménez J 2010 Hierarchy of minimal flow units in the logarithmic layer *Phys. Fluids* **22** 071704
- [30] Millikan C B 1938 A critical discussion of turbulent flows in channels and circular pipes *Proc. 5th Int. Conf. on Applied Mechanics* (New York: Wiley) pp. 386–92.